Hindawi
Journal of Nanomaterials
Volume 2020, Article ID 3541797, 12 pages
https://doi.org/10.1155/2020/3541797

Research Article

Bisphenol A Removal through Low-Cost Kaolin-Based Ag@TiO_2 Photocatalytic Hollow Fiber Membrane from the Liquid Media under Visible Light Irradiation

Usman Shareef[1,2] **and Muhammad Waqas**[1]

[1]*Shanghai Key Laboratory of Multiphase Materials Chemical Engineering, Membrane Science and Engineering R&D Lab, Chemical Engineering Research Center, School of Chemical Engineering, East China University of Science and Technology, 130 Meilong Road, 200237 Shanghai, China*
[2]*Advanced Membrane Technology Research Center (AMTEC), School of Chemical and Energy Engineering, Universiti Teknologi Malaysia, 81310 Skudai, Johor, Malaysia*

Correspondence should be addressed to Usman Shareef; y10190182@mail.ecust.edu.cn

Received 10 March 2020; Revised 30 April 2020; Accepted 25 May 2020; Published 22 June 2020

Guest Editor: Andrei Ivanets

Removal of bisphenol A (BPA) from water has presented a major challenge for the water industry. In this work, we report the BPA separation properties of truly low-cost kaolin-based visible light-activated photocatalytic hollow fiber membranes. The ceramic hollow fiber support was successfully fabricated by phase inversion and sintering method, whereas Ag@TiO_2 photocatalyst was prepared by liquid impregnation method. Different factors that affected the BPA removal were thoroughly investigated, including Ag loading in TiO_2 catalyst and immersion time during dip coating method. A reference BPA (10 mgl^{-1}) was used to check the photocatalytic performance of Ag@TiO_2 photocatalysts and prepared membranes. Comprehensive characterization including X-ray diffraction (XRD), field emission scanning electron microscopy (FESEM), energy-dispersive X-ray (EDX/S), Brunner-Emmer-Teller (BET), and UV-Vis spectroscopy revealed altered morphological and physicochemical properties of the photocatalytic membrane. UV-Vis results exhibited that the extended absorption edge of Ag@TiO_2 photocatalyst was observed into the visible region that led to its maximum BPA removal of 93.22% within 180 min under visible light irradiation. The FESEM images of the prepared membranes evinced a significant change in the structural morphologies, and UV-Vis showed the absorption edge in the visible region owing to the coating of the Ag@TiO_2 photocatalyst on the surface of the membrane. The resultant membrane showed a significant photocatalytic performance in the degradation of BPA (90.51% within 180 min) in an aqueous solution under visible light irradiation. At inference, the prepared membrane can be considered a promising candidate for efficient removal of BPA.

1. Introduction

Endocrine-disrupting chemicals (EDCs), such as bisphenol A (BPA), in water can be removed by a benign technique such as photocatalysis [1]. Specifically, semiconductor photocatalysis has attracted interest since solar energy or visible energy is an infinite and ecologically friendly energy resource [2]. Moreover, it has been used effectively in the degradation of EDCs and natural organic matter previously [3–5]. BPA is a raw material for epoxy resins and polycarbonates, which can be detected in some consumer products. Its exposure has been linked to infertility, hormonal imbalance, heart disease, breast cancer, and premature birth [6].

Nowadays, the most extensively examined photocatalyst titanium dioxide (TiO_2) is still activated under UV light. The utilization of photocatalysis under visible light or sunlight has not been widely adopted. TiO_2 exists in the form of anatase (band gap energy 3.2 eV) and rutile (band gap energy 3.0 eV), respectively, and these band gaps make it UV responsive [7, 8]. Moreover, low quantum efficiency

and stability restrict its development [9, 10]. It has been manifested that metal doping, for example, with palladium (Pd), platinum (Pt), gold (Au), cupper (Cu), and silver (Ag) could narrow the band gap of a photocatalyst by changing its crystallinity and boosting its photocatalytic performance [11]. Liu et al. prepared a visible light-activated Cu@TiO_2 photocatalyst for the removal of dissolved organic nitrogen (DON) and showed 10% amplified removal of DON under a visible light-activated Cu@TiO_2 photocatalyst compared to a conventional TiO_2 system [9]. A Ag-doped TiO_2 photocatalyst was comprehensively studied for the degradation of an organic substrate, and the results evinced 78% faster degradation than nascent TiO_2 photocatalyst [12]. Despite outstanding benefits of visible light-activated photocatalysis, there are two major disadvantages of photocatalysis, namely, separating the catalyst from the suspension solution and catalyst loss. Various studies have addressed these problems through membranes [2, 13] and porous materials, such as activated carbon [14] and nickel foam [15].

Membrane technology can be a promising technique for removing organic pollutants, suspended solids, and bacteria from the water [16, 17]. Photocatalytic membranes (PMs), the technology of filtration with both membrane and photocatalysis, have been investigated because they may improve the degradation efficiency of EDCs [18, 19]. For instance, Song et al. prepared a TiO_2/PVDF membrane and displayed improved NOM removal efficiency with enhanced self-cleaning ability [16]. Shareef et al. fabricated the PESf/TiO_2 membrane by phase inversion and sintering method, showing the augmented BPA removal efficiency under visible light irradiation [20]. However, previous studies have been focused on fabricating the TiO_2-based polymeric membrane under UV light, which exhibited polymer aging and could not stand harsh conditions.

Herein, novel low-cost kaolin-based visible light-activated Ag@TiO_2 photocatalytic hollow fiber membranes (Ag@TiCHFs) were prepared by the promising dip coating method for a highly efficient removal of bisphenol A (BPA). The effects of Ag loading (0.5, 0.8, 1.1, and 1.4 g) in TiO_2 catalyst and immersion time (0.5, 1.0, 1.3, and 2.0 min) during coating, on the degradation of BPA through the Ag@TiO_2 photocatalyst and the prepared membrane, were investigated thoroughly. The physiochemical properties of both the Ag@TiO_2 photocatalyst and prepared membrane were evaluated by different characterization (XRD, BET, UV-Vis spectrometry, FESEM, BET, and TOC) techniques. BPA (10 mgl^{-1}) as a pseudotenacious chemical was adopted to test the photocatalytic performance. Meanwhile, a Xenon lamp (100 W) was utilized as the light source to irradiate the visible light photocatalyst/composite membrane. The effects of Ag loading on TiO_2 catalyst and immersion time during coating on the membrane showed 93.21% and 90.51% BPA removal, respectively.

2. Experimental

2.1. Chemicals and Materials. The ceramic support was prepared from abundantly available kaolin ($Al_2H_4O_9SiO_2$, MW = 258.16 g/mole, Aldrich). N-methyl-2-pyrrolidone (NMP, solvent) and Arlacel P135 (dispersant) were purchased from Croda International Chemicals Ltd., UK. Polyether sulfone ($C_{12}H_8O_3$, PES, A300, AMECO Performance Product, USA) was used as a polymer binder. Deionized water (DI) was used as an external and internal coagulant during the spinning process. Ag@TiO_2 photocatalysts were synthesized from two materials: anatase (P25 Degusa TiO_2, purity ≥ 99%, BG = 3.2 eV) and silver nitrate ($AgNO_3$, purity ≥ 98%, Merck KGaA, Germany). Bisphenol A (BPA, purity ≥ 99%) was delivered by Sigma-Aldrich, and it was used as an EDC. All chemicals were used as received without purifications.

2.2. Preparation of Ag@TiO_2 Nanoparticles. The Ag@TiO_2 nanoparticles were prepared by the liquid impregnation method according to a previous report [20]. Firstly, 3.0 g of TiO_2 and 100 ml of DI water were mixed in a 500 ml conical flask to make TiO_2 suspension. After that, based on prior literature silver nitrate (0.5, 0.8, 1.1, and 1.4 g) was added into the suspension and the samples were designated as P-0 (neat TiO_2), P-1 (0.5 Ag@TiO_2), P-2 (0.8 Ag@TiO_2), P-3 (1.1 Ag@TiO_2), and P-4 (1.4 Ag@TiO_2), respectively. Homogenous slurry was obtained after 6 h continuous stirring with a magnetic stirrer. The homogenized slurry was dried at 90°C in an air oven for 10 h to make sure all the remaining water was removed followed by grinding with agate mortar to get fine particles. In the end, the fine particles were calcined at 400°C for 6 h in a muffle furnace. Fig. S1 and Table S1 in supplementary information (SI) illustrate the complete process for the preparation of Ag@TiO_2 nanoparticles.

2.3. Fabrication of Ceramic Hollow Fiber Support (CHF). α-Alumina is used as a main material for the fabrication of ceramic membranes [9]. However, it is expensive and a high sintering temperature is needed. Hence, to overcome these issues, current research is focused on cheaper materials like dolomite, clay, and kaolin for the fabrication of a membrane [10]. In the fabrication of a ceramic membrane, kaolin is extensively used as the foremost constituent. The fabrication of hollow fiber ceramic membrane (CHF) followed the method similar to a previous work [20]. Briefly, for the preparation of a casting solution, NMP, Aracel, and PESf were dissolved in the mass ratio of 42.5 : 1 : 6.5. A homogeneous polymer solution was obtained after stirring for 48 h. Moreover, 50 wt% of kaolin was mixed in the solution and stirred for the next 48 h. The ceramic supports were obtained by spinning the casting solution through tubes in an orifice spinneret. DI water was used for the phase inversion and ceramic supports were sintered at 1400°C for 24 h in a muffle furnace. The membranes were kept in a DI water to remove the remaining NMP and dried at 70°C before use. The spinning parameters and casting solution composition are given in Table S2 in SI.

2.4. Preparation of Ag@TiO_2 Modified Ceramic Hollow Membrane (Ag@TiCHFs). The Ag@TiO_2 nanoparticles were deposited on the hollow fiber ceramic membrane via the dip coating technique (Fig. S2 in SI). Briefly, 0.6 g of Ag/TiO_2

nanoparticles was dissolved in 400 ml of DI water followed by sonication for 1 h. Moreover, an epoxy resin was used to close both ends of CHF and potted on the adapter for overnight drying at room temperature. After that, the CHF having the length of 15 cm was dipped into the $Ag@TiO_2$ solution for different immersion times (IT = 0.5, 1.0, 1.3, and 2 min) and then dried at ambient temperature for 20 h. The resultant membranes (PM-0: pristine membrane; PM-1: IT = 0.5 min Ag@TiCHF; PM-2: IT = 1 min Ag@TiCHF; PM-3: IT = 1.3 min Ag@TiCHF; and PM-4: 2 min Ag@TiCHF) were sintered at 500°C for 2 h (2°C per minute).

2.5. Characterizations

2.5.1. Morphology. The surface morphology of the pristine membrane and the Ag@TiCHF membranes was observed by field emission scanning electron microscopy (FESEM, Quanta 200F, FEI) coupled with energy-dispersive X-ray analysis (EDX) for elemental analysis. The Brunauer-Emmet-Teller (BET Quanta chrome Autosorb-1 MP) was used to investigate the surface area of $Ag@TiO_2$ photocatalysts. X-ray diffraction (XRD-6000, Cu Kα radiation, Shimadzu Lab, Japan) was used to get the crystallinity of the pristine membrane and Ag@TiCHF membrane followed by the UV-Vis spectrometry (UV-2000, Shimadzu, Japan) analysis for optical properties. Finally, concentration of total organic carbon (TOC) in the solution was measured using a TOC analyzer (Shimadzu, Kyoto, Japan). The TOC was determined as the difference between total carbon (TC) and inorganic carbon (IC).

The band gap energy of $Ag@TiO_2$ photocatalysts and Ag@TiCHF membranes was calculated by the following correlations.

$$E = h\nu, \tag{1}$$

$$\lambda = \frac{1240}{E}, \tag{2}$$

$$E(\text{eV}) = \frac{1240}{\lambda}. \tag{3}$$

2.5.2. Pure Water Flux (PWF) and BPA Rejection. The separation performance of the pristine membrane and Ag@TiCHF membranes was examined using a pilot scale crossflow filtration device (Fig. S3 in SI). Prior to calculating the flux, the membrane samples were immersed in deionized water at 1.0 bar for 0.5 h to reach a uniform state, and then pressure was amended to 2.0 bar. The pure water flux and rejection (R) of BPA were calculated through the following equations.

$$\text{PWF} = \frac{V}{A \times \Delta t}. \tag{4}$$

Here, V is the volume (l) of water permeated during the experiment, A is the effective area (m^2) of the membrane, and Δt is the filtration time (h).

$$R = \left[1 - \frac{C_P}{C_F}\right] \times 100, \tag{5}$$

where C_p is the BPA concentration in permeate and C_f is the concentration in the feed. The rejection of BPA was tested in 100 mgl^{-1} of feed solution.

2.6. The Assessment of Photocatalytic Performance

2.6.1. The Photocatalytic Performance of $Ag@TiO_2$ Photocatalyst. The performance of the pure TiO_2 and $Ag@TiO_2$ photocatalysts was investigated using a photocatalytic reactor coupled with a 100 W Xe lamp used for irradiation (Fig. S4 in SI). The photocatalytic reactor (250 ml) contains 0.2 wt. % $Ag@TiO_2$ photocatalyst and 10 mgl^{-1} of BPA solution. To confirm the adsorption equilibrium of BPA on the catalyst, the solution was mixed in the dark for 30 min followed by a continuous reaction under a light source. To test the BPA concentration, samples were taken from the solution at certain time intervals (after 0.5 h), which were tested for absorbance of BPA at 276 nm using a UV-Vis spectrophotometer.

2.6.2. The Photocatalytic Performance of Ag@TiCHF Membrane. The photocatalytic performance of a pristine membrane and Ag@TiCHF membranes was determined in the photocatalytic reactor (fig. S4 in SI). The reactor was attached with a Xe lamp (100 W), which acts as a light source for irradiation. In addition, the membrane (7.0 cm) was drenched in the solution (100 ml, BPA 10 mgl^{-1}) and stirred for 0.5 h in the dark followed by continuous stirring under the Xe lamp for photocatalytic reaction. The sample was taken from every 0.5 h to be tested for BPA concentration.

3. Results and Discussion

3.1. The Effect of Ag Loading in the Properties of $Ag@TiO_2$ Photocatalyst

3.1.1. Surface Morphology. Figure 1 illustrates the FESEM images of neat TiO_2 and $Ag@TiO_2$ photocatalysts. According to images, the amount of Ag observed on the surface of the TiO_2 photocatalyst in the white spot, increased with increasing Ag concentration, leading to the aggregation on the surface. Moreover, the Ag was not uniformly distributed on the TiO_2 surface [21]. In addition, the $Ag@TiO_2$ photocatalyst presented as irregular-shaped aggregates composed of smaller Ag particles [22]. The aggregation amplified with increasing the concentration of Ag loading from 0.5 g to 1.4 g, as confirmed by EDX analysis. The aggregation is more prominent in the P-4 (1.4 g $Ag@TiO_2$) sample, and this may tremendously reduce the band gap of TiO_2 and consequently improved photocatalytic removal efficiency [23]. The EDX analysis of P-4 (Figure 2) demonstrated that Ag is not uniformly dispersed on the surface of TiO_2, which is in accordance with previous works [24, 25]. The elemental compositions of $Ag@TiO_2$ photocatalysts are shown in Table S3 in SI, which exhibited lower amount of Ag than the targeted amount. One possible reason could be sequestrated $AgNO_3$ during annealing in the furnace. This

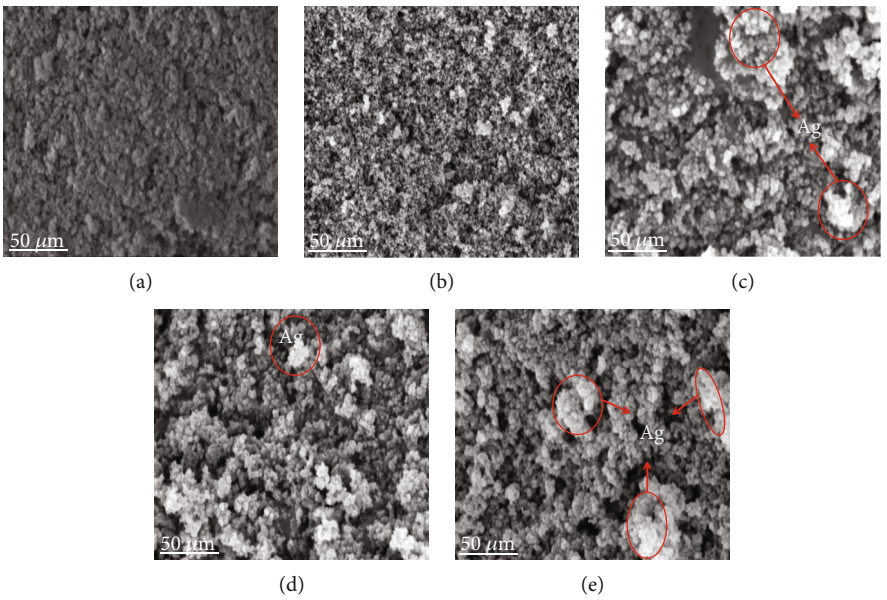

Figure 1: FESEM images of Ag@TiO_2 photocatalysts: (a) P-0 (neat TiO_2), (b) P-1 (0.5 g Ag@TiO_2), (c) P-2 (0.8 g Ag@TiO_2), (d) P-3 (1.1 g Ag@TiO_2), and (e) P-4 (1.4 g Ag@TiO_2).

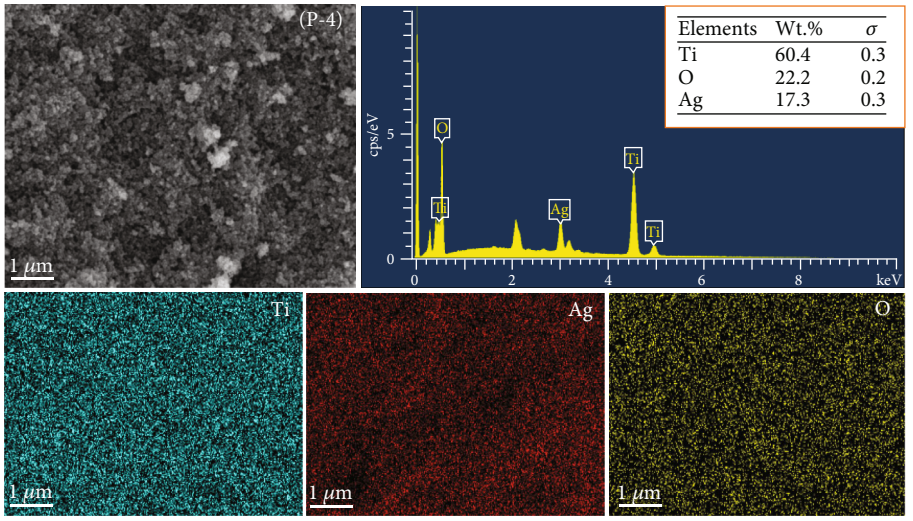

Figure 2: EDX analysis of P-4 (1.4 g Ag@TiO_2).

confirms the unequal distribution of Ag followed by the absence extraneous roots, which agrees with the FESEM result. Minor traces of vanadium were also observed in the graph owing to impurities from FESEM analysis. The assumption is based on the fact that there was no peak of impurity on the XRD patterns.

3.1.2. Crystalline Properties. The XRD results in Figure 3 evinced that all Ag@TiO_2 samples are composed of anatase with the (101) characteristic peak established at 25.25° corresponding to ICDD-PDF (01-089-0553) followed by other small peaks at 37.4°, 47.0°, 54.0°, 63.12°, 69.8°, 71.31°, and 74.8°, agreeing to planes (1 1 3), (2 0 1), (2 1 2), (2 0 5), (1 1 7), (2 2 1), and (3 0 2), respectively (JSPD 01-079-3104) [26]. However, the rutile peaks start from 26.37°, 38.02°, 40.34°, 44.89°, 55.28°, 55.5°, and 88.3°, which correspond to the diffractions planes (1 1 0), (2 0 0), (1 1 1), (2 1 0), (2 1 1), and (2 2 0) with JSPD card no. 01-079-1543. Moreover, Ag peaks were observed at 20.57°, 22.53°, and 25.21° with the diffraction plans (1 1 1), (2 0 1), and (0 2 0) accordingly (JSPD card no. 01-073-4889). It has been reported that Ag mixing in TiO_2 does not have an effect on the structure of anatase, showing that the silver dopant is not uniformly distributed on the surface of TiO_2, which is in agreement with FESEM and EDX [27].

Debye Scherrer's formula was used to calculate the crystal size of all the samples [28].

$$D = \frac{0.94\lambda}{\beta \cos \theta}. \quad (6)$$

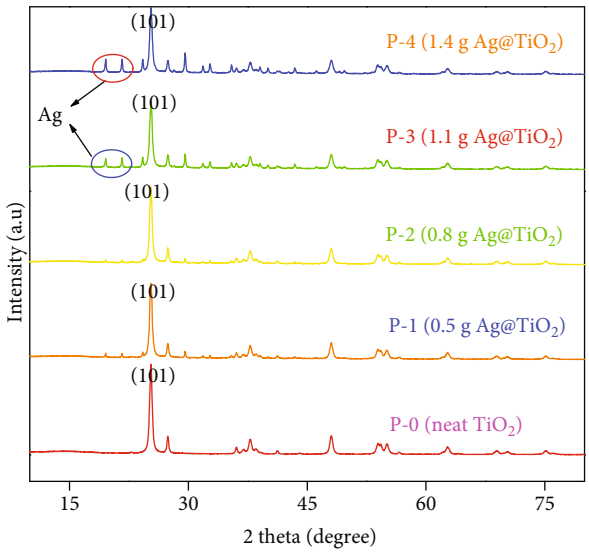

Figure 3: The XRD peaks of $Ag@TiO_2$ photocatalysts.

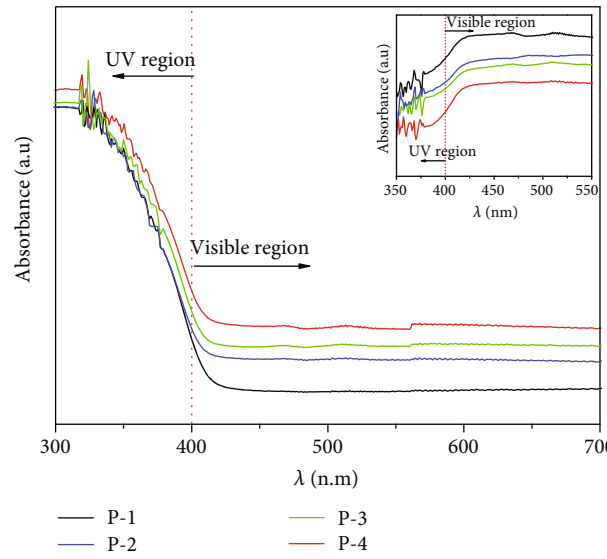

Figure. 4: Absorption curves of $Ag@TiO_2$ photocatalysts (P-1 =0.5 g $Ag@TiO_2$, P-2 = 0.8 g $Ag@TiO_2$, P-3 =1.1 g $Ag@TiO_2$, and P-4 =1.4 g $Ag@TiO_2$). Inset: broad absorption between 350 and 550 nm.

Here λ, θ, and β is the wavelength, Bragg's angle, and FWHM (full-width half-maximum), respectively. The results are demonstrated in Table S4 in SI. It was observed that the grain size of all $Ag@TiO_2$ samples elevated from 28.81 to 50.22 nm corresponding to increased Ag concentration. The variations in grain size were noticed with the change in deposition time which affected the photocatalytic efficiencies of the membrane [28].

3.1.3. BET Analysis. The BET surface area (S_a) of neat TiO_2 and $Ag@TiO_2$ photocatalysts was calculated by N_2 adsorption-desorption isotherms. The isotherms manifested a hysteresis loop, which confirmed the mesoporous characteristic of the materials [29]. The BET surface area along with the crystal size of all the samples is listed in Table S4 in SI. The results in Table S4 and Figure S5 showed that changing the concentration of Ag from 0.5 to 1.4 g in the TiO_2 solution gradually reduces the surface area owing to the deposition of Ag aggregates on the surface of TiO_2 catalyst, leading to pore blocking [22], which confirms both FESEM and XRD results. Hence, for the P-3 sample, the surface area, pore volume (V_p), and pore diameter decreases in size as the amount of Ag deposition increases, reaching 31.747 m^2/g, 0.214526 cm^3/g, and 7.8 nm, respectively. This may be because Ag clusters block the TiO_2 capillaries [30].

3.1.4. UV-Vis-NIR Diffuse Reflectance Spectroscopic Measurement. Figure 4 shows the absorption curves of $Ag@TiO_2$ photocatalyst estimated by UV-Vis-NIR spectroscopic measurement. The photocatalysts appear as the sharp edge in the visible region at about 427 nm [31]. Moreover, there is no change observed in the absorption edge with the addition of different amounts of Ag in the TiO_2 catalyst, leading to the distinctive plasmon absorption of Ag at 400 to 500 nm slowly mixed up and amplified in correlation with Ag content, exhibiting the aggregation of Ag on the surface of TiO_2 catalyst [32]. The Kubelka-Munk function was used to calculate the band gap of all the $Ag@TiO_2$ samples. The band gaps of all the samples are given in Table S4 in SI. The broad absorption observed between 350 and 550 nm (Figure 4 inset) is possibly because of the enhancement of absorption of the visible light harvesting [33]. Notably, when the Ag concentration is increased up to 1.4 g (P-4, $Ag@TiO_2$), an increase is observed in the wavelength value, because of bigger size Ag clusters present on the surface of TiO_2, which confirms with FESEM results. Therefore, P-4 sample with the concentration of 1.4 g was selected for the coating.

3.2. The Effect of Immersion Time of $Ag@TiO_2$ Photocatalyst in the Properties of Ceramic Hollow Fiber Membrane

3.2.1. Morphology of Ag@TiCHF Membrane. Figure 5 showed the FESEM images of Ag@TiCHF membranes demonstrating that $Ag@TiO_2$ photocatalyst were successfully deposited on the surface of ceramic hollow fiber membranes, and the EDX graph (Figure 6, PM-4: IT = 2 min) confirmed the existence of Ag, O, and Ti on the porous CHF, while mapping exhibited the uniform dispersion on the surface. Teow et al. found similar results while preparing the TiO_2-doped mixed matrix membrane [34]. Moreover, the thickness/layer of the $Ag@TiO_2$ photocatalyst on the porous surface depends on the immersion time in the soaking of the ceramic hollow fiber membrane into the photocatalyst solution, and it can be visualized more vividly by increasing the immersion time [7]. Therefore, there are few $Ag@TiO_2$ nanoparticles on the surface of the PM-1 membrane (Figure 6(d)) compared to PM-2 (Figure 6(f)), PM-3 (Figure 6(h)), and PM-4 (Figure 5(j)), respectively. This indicates higher aggregation on the surface with the increase of the immersion time from 0.5 to 2.0 min, leading to pore blocking of membranes which might affect the pure water flux and photocatalytic efficiency of the membranes.

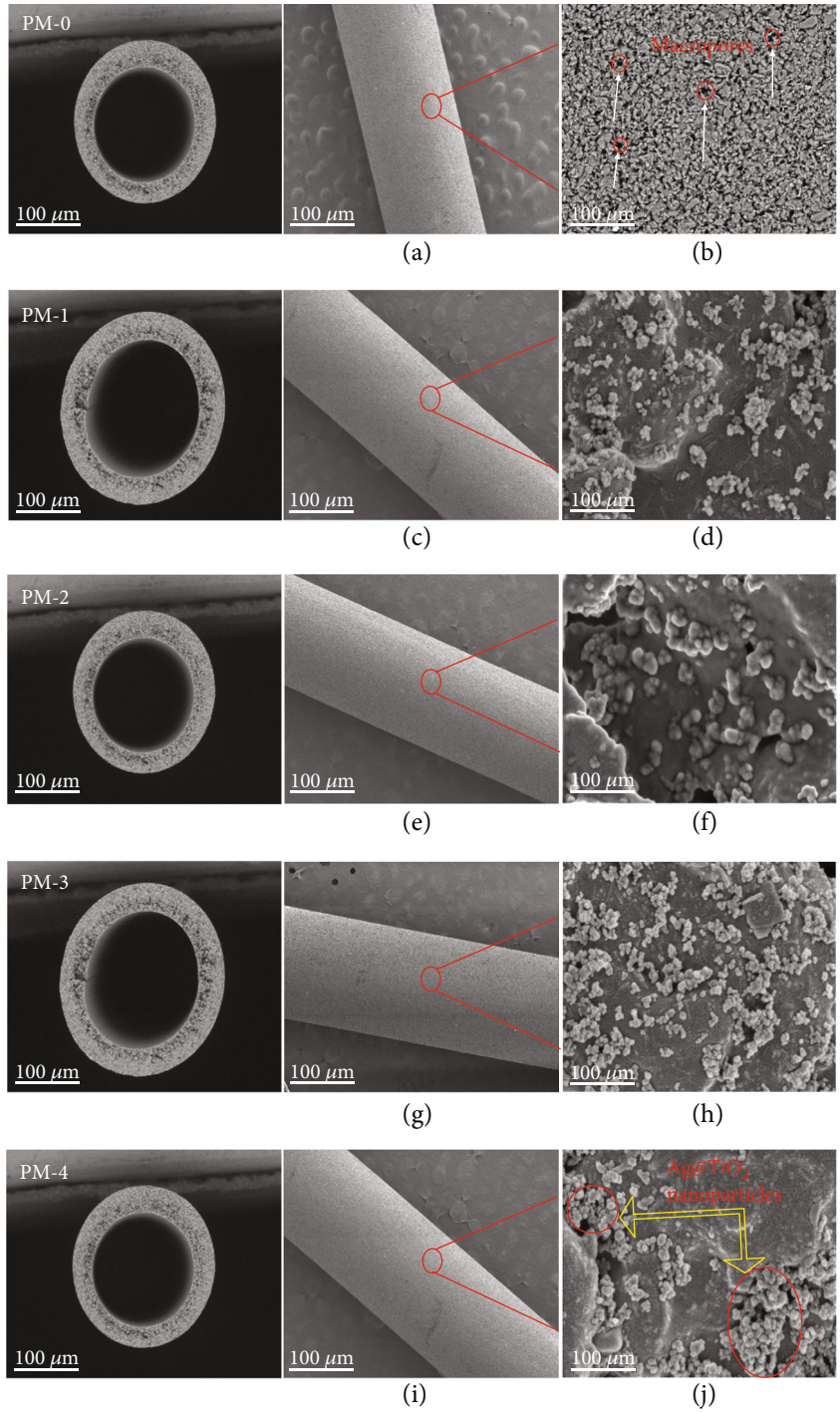

Figure 5: FESEM images of Ag@TiCHF membranes, PM-0 (pristine membrane), P-1 (IT = 0.5 min), PM-2 (IT = 1 min), PM-3 (IT = 1.3 min), and PM-4 (IT = 2 min).

3.2.2. Structure Analysis of Ag@TiCHF Membrane. Figure 7 manifests the clear XRD graphs of the Ag@TiO_2 photocatalyst, pristine membrane, and Ag@TiCHF membranes, respectively. The kaolinite peaks of pristine membrane (PM-0) were seen at 2θ of 9.48°, 15.9°, 24.32°, and 26.18° with planes (1 1 0), (1 2 0), (1 1 1), and (1 2 1) confirmed by JCPDS card No. 01-0791456 [35]. As Ag@TiO_2 photocatalyst was deposited on the surface of CHFs, the peaks slightly shifted from 15.9° to 26.0° to higher intensity with the difference of 10.1° of 2-theta. These variations in peaks may be caused by the augmented aggregation of the Ag@TiO_2 photocatalyst on the surface [35, 36]. In addition, as the immersion time increased from 0.5 to 2 min during deposition, the nanoparticles became more agglomerated, which is in accordance

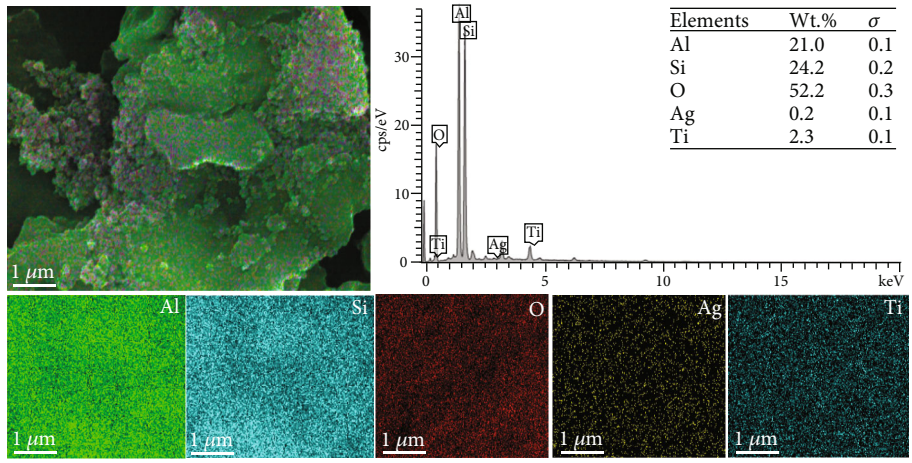

Elements	Wt.%	σ
Al	21.0	0.1
Si	24.2	0.2
O	52.2	0.3
Ag	0.2	0.1
Ti	2.3	0.1

Figure 6: EDX and mapping of the PM-4 membrane.

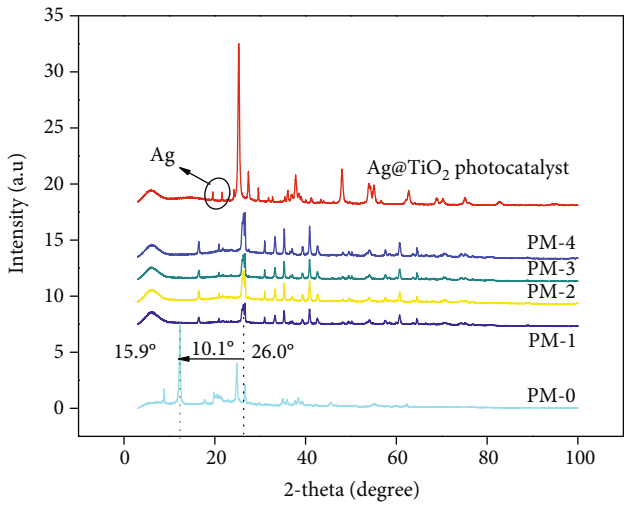

Figure 7: XRD patterns of Ag@TiCHF membranes, PM-0 (pristine membrane), P-1 (IT = 0.5 min), PM-2 (IT = 1 min), PM-3 (IT = 1.3 min), PM-4 (IT = 2 min), and Ag@TiO_2 photocatalyst.

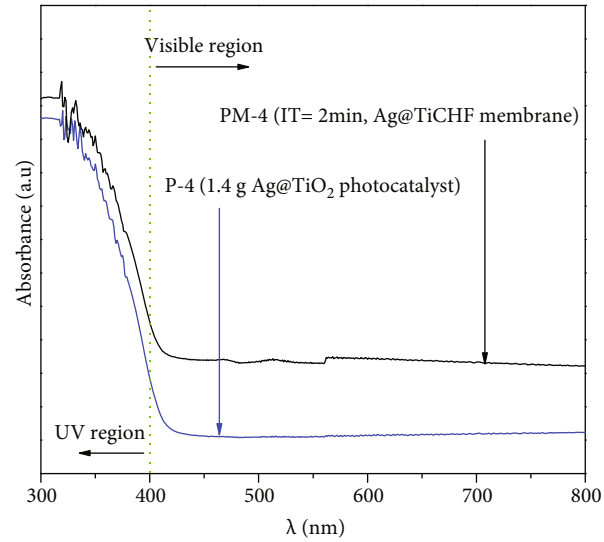

Figure 8: UV-Vis curves of PM-4 (IT = 2 min, Ag@TiCHF membrane) and P-4 (1.4 g Ag@TiO_2) photocatalyst.

with FESEM results. Moreover, Figure 8 also displays the peaks of the Ag@TiO_2 photocatalyst with obvious peaks of anatase at 10.5°, 20.7°, 31.8°, and 51.2° in accordance with JSPD card no. 01-083-0471 also indicating the silver peaks at 43.4° and 63.6° (JCPDS card no. 02-0821), respectively.

3.2.3. Optical Properties. The absorbance spectra of Ag@TiO_2 photocatalyst (P-4, 1.4 g Ag@TiO_2) and Ag@TiCHF membrane (PM-4, IT = 2 min) from the UV diffuse reflection spectrometer are displayed in Figure 8, indicating the large absorption edge of the coated membrane, which is a characteristic of its sound removal performance of BPA under the Xe light. Figure 8 also showed the absorption edge of the photocatalyst at about 420 nm. It has been reported that the structural defect of crystal lattice and variation in energy level might be caused by doping Ag; therefore, the absorption edge has varied and reduced the band gap [37, 11], which is calculated by the equation stated previously [38] and reported in Table S4 in SI. Narrowing the band gap of the Ag@TiCHF membrane exhibited that the Ag@TiO_2 photocatalyst was more agglomerated on the surface of the membrane with increased immersion time, which agrees with the FESEM results (Figure 6(h)).

3.2.4. Pure Water Flux. The pure water flux (PWF) of the pristine membrane and Ag@TiCHF membranes is exhibited in Figure 9. The PWF decreased significantly with the increase of the immersion time from 0.5 to 2 min during the coating of Ag@TiO_2 nanoparticles on the ceramic membranes. One possible description of this inference could be the accumulation of the photocatalyst on the surface as increasing the immersion time. These results are similar with the literature reported in the literature [39, 40]. On the other hand, higher amount of nanoparticles on the porous surface can lead to pore blocking due to the existence of macropores on the surface, as can be seen on the FESEM images (Figure 6(b)) consequently reducing the pure water flux [41].

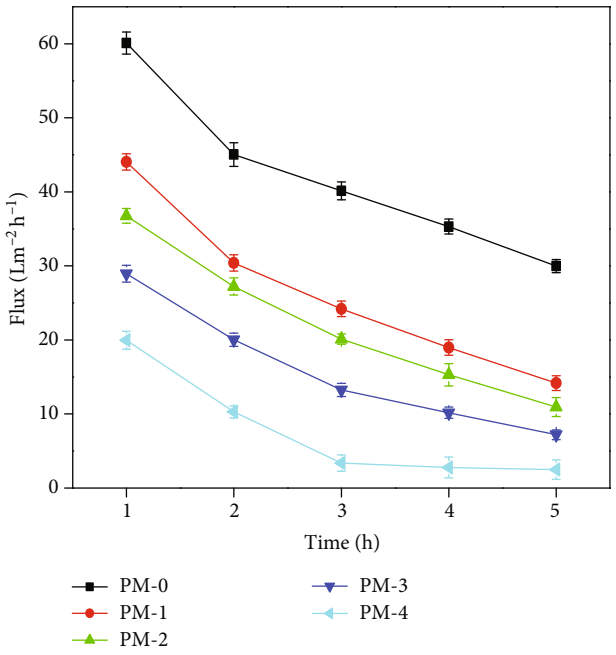

Figure 9: Effect of immersion time on pure water flux of Ag@TiCHF membranes.

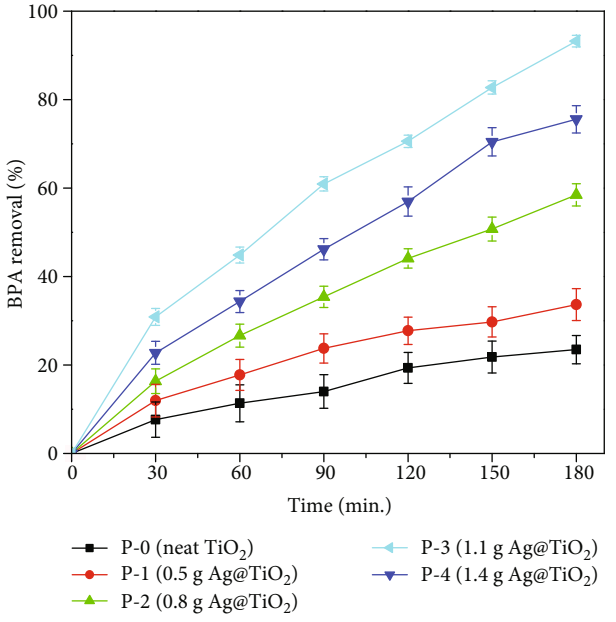

Figure 10: The effects of Ag loading on the BPA removal efficiency of TiO_2 catalyst under visible light irradiation.

3.3. Photocatalytic Performance

3.3.1. Effect of Immersion Time on the Performance of BPA Removal. The effects of Ag loading on TiO_2 catalyst for BPA removal under visible light irradiation is displayed in Figure 10. Sample P-3 (1.1 g Ag@TiO_2 photocatalyst) showed the highest BPA removal efficiency of the photocatalysts tested, achieving 93.21% removal under visible light irradiation. Higher Ag loading leads to higher BPA removal capability, as expected and seen in the photocatalysts P-0 to P-3. However, it appears that higher amount of Ag loading becomes inhibitory to photocatalytic activity, as can be seen in the reduction in performance from P-3 to P-4, despite the increase in Ag loading. The extra silver ions present on the surface of TiO_2 could decrease its photocatalytic and charge separation efficiency by spinning into another recombination center of electron-hole sets [42]. In addition, By comparing the TOC values for TiO_2 modified with varying amounts of silver (Table S5), it can be clearly observed that the reduction in the TOC value in the presence of P-3 (1.1 g Ag@TiO_2) is significantly higher than other samples. Based on the results presented in this section, the P-3 photocatalyst was identified as the optimal Ag loading that leads to the highest BPA degradation rate under visible light irradiation, hence chosen for coating on the ceramic membrane.

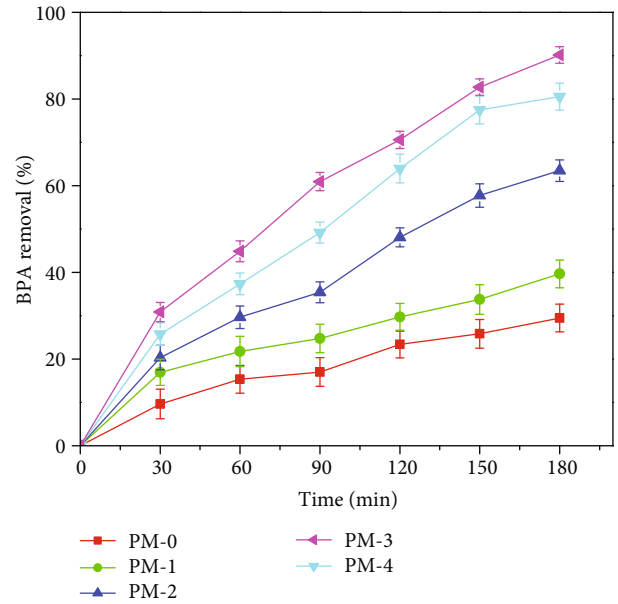

Figure 11: Effects of immersion time on the BPA removal efficiency of photocatalytic Ag@TiCHF hollow fiber membranes, PM-0 (pristine membrane), P-1 (IT = 0.5 min), PM-2 (IT = 1 min), PM-3 (IT = 1.3 min), and PM-4 (IT = 2 min).

3.3.2. Effect of Silver Loading on the Performance of BPA Removal. The photocatalytic properties of the pristine membrane and photocatalytic Ag@TiCHF membranes were evaluated by measuring the BPA degradation under visible light irradiation. Figure 11 shows that the photocatalytic membranes, each prepared with varying immersion time from 0.5 to 2 min as well as the neat membrane, manifested varying levels of degradation of BPA under the Xe lamp. The Ag@TiO_2-doped membranes showed the higher rate of degradation of BPA than the undoped membrane, and among the Ag@TiO_2-doped membranes, higher immersion time during their preparation correlate with higher BPA degradation. Higher immersion time can be construed to lead to a greater number of Ag@TiO_2 nanoparticles which is the responsible of the photocatalytic activity. A covalent linkage

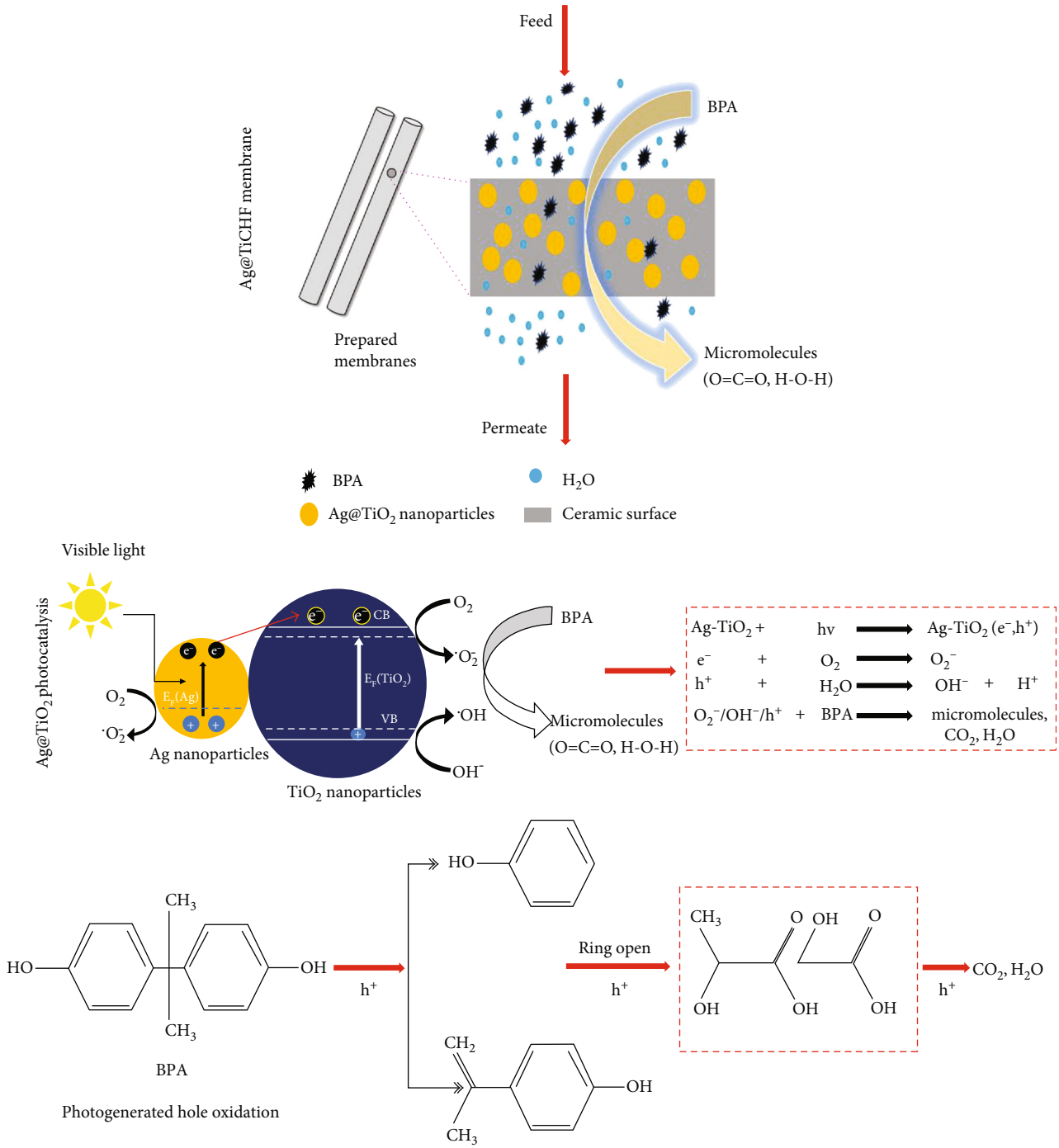

Figure 12: Mechanism of the Ag@TiCHF photocatalytic membrane for BPA removal under visible light irradiation.

might occur on the surface of the membrane that indicates the hydrogen bonding between nanoparticles and the membrane [43]. Figure 11 shows that the PM-3 membrane possesses the highest degradation of BPA (90.51%) under visible light irradiation. Nevertheless, when the immersion time is raised to 2.0 min, additional Ag@TiO_2 nanoparticles on the surface of the membrane exhibited major agglomeration, which decreased the number of active sites of the membrane leading to the reduction of BPA removal.

3.4. Possible BPA Degradation Mechanism by Ag@TiCHF Membrane. Figure 12 shows the possible BPA removal mechanism by the Ag@TiCHF membrane. Initially, BPA molecules rapidly agglomerate and penetrate into the porous surface through adsorption, after which the photocatalysis process takes place under visible light [42]. Doping silver ions into TiO_2 narrows its band gap by presenting impurity, causing the local states to lower the conduction band edge and shift its absorption frequency into the visible light region.

Table 1: Comparison with the available literature.

Membrane	Catalyst	Fabrication method	Light source	Investigated benefits	Ref.
PESf	TiO_2	Phase inversion	No photocatalysis	Stability and anti-fouling ability	[37]
PESf	TiO_2	Phase inversion	No photocatalysis	Hydrophilicity	[45]
PES	TiO_2	Surface modification	UV	High photocatalytic activity	[46]
PVDF	TiO_2	Phase inversion	UV	High antifouling ability and self-cleaning properties	[15]
PVDF	TiO_2	Phase inversion	UV	Hydrophilicity	[47]
Monolith	TiO_2	Dip coating	Vis/UV	High photocatalytic activity	[48]
Monolith	TiO_2/rGO	Dip coating	Vis	High photocatalytic activity	[49]
Alumina	TiO_2/rGO	Multilayer coating	UV	Antifouling ability	[50]
PSf	Fe/TiO_2	Phase inversion	Vis	High photocatalytic activity	[44]
Kaolin	Ag/TiO_2	Phase inversion	Vis	High BPA removal efficiency	This study

The Ag@TiO_2 nanoparticles inside the prepared membrane perform the separation of a photogenerated carrier under the Xe lamp. The electrons move from valence band to conduction band to create photoelectrons (e^-) and positive holes (h^+), which react with oxygen and water to produce $O_2^{\cdot-}$ and $^{\cdot}HO$ free radicals. These free radicals could breakdown BPA into CO_2 and H_2O [44].

3.5. Performance Comparison with Available Photocatalytic Membranes in Literature. Several membranes doped with different photocatalysts have been reported these days. Table 1 contains different membranes coated with different catalysts. The table is cataloged with membrane material, types of nanoparticles, fabrication method, investigated benefits, and source of light. According to Table 1, Ag@TiO_2 coating on the porous surface changes the morphology and enhances the separation performance of the membrane, whereas former researchers emphasize on the improvement in the hydrophilicity, PWF, and antifouling properties of the membrane. Also, their focus is to investigate the performance of TiO_2-doped photocatalytic polymer membrane under UV light, which will cause the polymer degradation in the long-term operation. Ceramic membrane with good physiochemical and mechanical properties can perform under harsh conditions, but a high price restricts its extensive applications. In this study, the Ag@TiO_2 photocatalytic membrane was fabricated by the dip coating method and performed under visible light which led to the degradation of BPA up to 90% under visible light irradiation. Therefore, this membrane can be the prime candidate for the removal of EDCs from the liquid media.

4. Conclusion

In this research, Ag@TiO_2 photocatalytic ceramic hollow fiber membranes (Ag@TiCHF) were prepared by dip coating method. The effects of Ag loading on BPA removal efficiency of Ag@TiO_2 photocatalysts were studied comprehensively. In addition, the influence of immersion time of Ag@TiO_2 nanoparticles on the surface of ceramic membrane during dip coating method was discussed in detail. The FESEM results of the membranes indicated the deposition of Ag@TiO_2 nanoparticles on the ceramic membrane, and UV-Vis confirmed the absorption edge in the visible region. In addition, the coating of nanoparticles on the ceramic surface enabled the membrane to perform visible light photocatalysis and separation simultaneously. The membrane containing 1.1 g Ag@TiO_2 photocatalyst with immersion time 1.3 min displayed the highest BPA removal under visible light irradiation. Hence, these photocatalytic membranes are considered for the removal of carcinogenic chemicals from the water.

Data Availability

All data generated or analysed during this study are included within the article (and its supplementary information file).

Conflicts of Interest

The authors declare that they have no conflicts of interest.

Acknowledgments

The authors would like to thank Research Management Centre, Universiti Teknologi Malaysia and Chemical Engineering Research Center, East China University of Science and Technology for the technical support.

Supplementary Materials

Figure S1: illustration of Ag@TiO_2 nanoparticles. Figure S2: modification of ceramic hollow fiber membrane. Figure S3: pure water flux calculation of membrane device. Figure S4: photocatalytic reactor. Figure S5: BET graphs of Ag@TiO_2 nanoparticles. Table S1: composition for the preparation of Ag@TiO_2 nanoparticles. Table S2: the spinning parameters and casting solution compositions. Table S3: elemental composition of Ag in TiO_2 catalyst. Table S4: the grain size, surface area, and band gap of Ag@TiO_2 photocatalysts. Table S5: reduction in the TOC value (%) of BPA solution using Ag/TiO_2 photocatalysts. *(Supplementary Materials)*

References

[1] K. M. Lee, C. W. Lai, K. S. Ngai, and J. C. Juan, "Recent developments of zinc oxide based photocatalyst in water treatment

technology: a review," *Water Research*, vol. 88, pp. 428–448, 2016.

[2] S. Leong, A. Razmjou, K. Wang, K. Hapgood, X. Zhang, and H. Wang, "TiO_2 based photocatalytic membranes: a review," *Journal of Membrane Science*, vol. 472, pp. 167–184, 2014.

[3] J. P. Méricq, J. Mendret, S. Brosillon, and C. Faur, "High performance PVDF-TiO_2 membranes for water treatment," *Chemical Engineering Science*, vol. 123, pp. 283–291, 2015.

[4] Y. Shi, J. Huang, G. Zeng, W. Cheng, and J. Hu, "Photocatalytic membrane in water purification: is it stepping closer to be driven by visible light?," *Journal of Membrane Science*, vol. 584, pp. 364–392, 2019.

[5] D. K. Wang, M. Elma, J. Motuzas, W. C. Hou, F. Xie, and X. Zhang, "Rational design and synthesis of molecular-sieving, photocatalytic, hollow fiber membranes for advanced water treatment applications," *Journal of Membrane Science*, vol. 524, pp. 163–173, 2017.

[6] S. Yüksel, N. Kabay, and M. Yüksel, "Removal of bisphenol A (BPA) from water by various nanofiltration (NF) and reverse osmosis (RO) membranes," *Journal of Hazardous Materials*, vol. 263, pp. 307–310, 2013.

[7] H. Dzinun, M. H. D. Othman, A. F. Ismail, M. H. Puteh, M. A. Rahman, and J. Jaafar, "Morphological study of co-extruded dual-layer hollow fiber membranes incorporated with different TiO_2 loadings," *Journal of Membrane Science*, vol. 479, pp. 123–131, 2015.

[8] M. Inagaki, R. Nonaka, B. Tryba, and A. W. Morawski, "Dependence of photocatalytic activity of anatase powders on their crystallinity," *Chemosphere*, vol. 64, no. 3, pp. 437–445, 2006.

[9] C. Liu, J. Wang, W. Chen, C. Dong, and C. Li, "The removal of DON derived from algae cells by Cu-doped TiO_2 under sunlight irradiation," *Chemical Engineering Journal*, vol. 280, pp. 588–596, 2015.

[10] A. Petala, Z. Frontistis, M. Antonopoulou, I. Konstantinou, D. I. Kondarides, and D. Mantzavinos, "Kinetics of ethyl paraben degradation by simulated solar radiation in the presence of N-doped TiO_2 catalysts," *Water Research*, vol. 81, pp. 157–166, 2015.

[11] H. R. Rajabi, O. Khani, M. Shamsipur, and V. Vatanpour, "High-performance pure and Fe^{3+}-ion doped ZnS quantum dots as green nanophotocatalysts for the removal of malachite green under UV-light irradiation," *Journal of Hazardous Materials*, vol. 250-251, pp. 370–378, 2013.

[12] L. M. Santos, W. A. Machado, M. D. França et al., "Structural characterization of Ag-doped TiO_2 with enhanced photocatalytic activity," *RSC Advances*, vol. 5, no. 125, pp. 103752–103759, 2015.

[13] E. Bet-moushoul, Y. Mansourpanah, K. Farhadi, and M. Tabatabaei, "TiO_2 nanocomposite based polymeric membranes: a review on performance improvement for various applications in chemical engineering processes," *Chemical Engineering Journa*, vol. 283, pp. 29–46, 2016.

[14] B. Gao, P. S. Yap, T. M. Lim, and T. T. Lim, "Adsorption-photocatalytic degradation of Acid Red 88 by supported TiO_2: effect of activated carbon support and aqueous anions," *Chemical Engineering Journal*, vol. 171, no. 3, pp. 1098–1107, 2011.

[15] S. Qiu, S. Xu, G. Li, and J. Yang, "Synergetic effect of ultrasound, the heterogeneous fenton reaction and photocatalysis by TiO_2 loaded on nickel foam on the degradation of pollutants," *Materials (Basel)*, vol. 9, no. 6, p. 457, 2016.

[16] H. Song, J. Shao, Y. He, B. Liu, and X. Zhong, "Natural organic matter removal and flux decline with PEG- TiO_2-doped PVDF membranes by integration of ultrafiltration with photocatalysis," *Journal of Membrane Science*, vol. 405-406, pp. 48–56, 2012.

[17] S. Mozia, D. Darowna, R. Wróbel, and A. W. Morawski, "A study on the stability of polyethersulfone ultrafiltration membranes in a photocatalytic membrane reactor," *Journal of Membrane Science*, vol. 495, pp. 176–186, 2015.

[18] O. Iglesias, M. J. Rivero, A. M. Urtiaga, and I. Ortiz, "Membrane-based photocatalytic systems for process intensification," *Chemical Engineering Journal*, vol. 305, pp. 136–148, 2016.

[19] X. Zhang, D. K. Wang, and J. C. Diniz Da Costa, "Recent progresses on fabrication of photocatalytic membranes for water treatment," *Catalysis Today*, vol. 230, pp. 47–54, 2014.

[20] U. Shareef, M. H. D. Othman, A. F. Ismail, and A. Jilani, "Facile removal of bisphenol A from water through novel Ag-doped TiO_2 photocatalytic hollow fiber ceramic membrane," *Journal of the Australian Ceramic Society*, vol. 56, no. 1, pp. 29–39, 2020.

[21] S. Khan, I. A. Qazi, I. Hashmi, M. A. Awan, and N. U. S. S. Zaidi, "Synthesis of silver-doped titanium TiO_2 powder-coated surfaces and its ability to inactivate *pseudomonas aeruginosa* and *bacillus subtilis*," *Journal of Nanomaterials*, vol. 2013, Article ID 531010, 8 pages, 2013.

[22] N. Sobana, M. Muruganadham, and M. Swaminathan, "Nano-Ag particles doped TiO_2 for efficient photodegradation of Direct azo dyes," *Journal of Molecular Catalysis A: Chemical*, vol. 258, no. 1-2, pp. 124–132, 2006.

[23] H. Ilyas, I. A. Qazi, W. Asgar, M. A. Awan, and Z. U. D. Khan, "Photocatalytic degradation of nitro and chlorophenols using doped and undoped titanium dioxide nanoparticles," *Journal of Nanomaterials*, vol. 2011, Article ID 589185, 8 pages, 2011.

[24] H. Younas, I. A. Qazi, I. Hashmi, M. A. Awan, A. Mahmood, and H. A. Qayyum, "Visible light photocatalytic water disinfection and its kinetics using Ag-doped titania nanoparticles," *Environmental Science and Pollution Research International*, vol. 21, no. 1, pp. 740–752, 2014.

[25] Y. Li, Y. Guo, and Y. Liu, "Synthesis of high purity TiO_2 nanoparticles from $Ti(SO_4)_2$ in presence of EDTA as complexing agent," *China Particuology*, vol. 3, no. 4, pp. 240–242, 2005.

[26] M. S. Abdel-wahab, A. Jilani, I. S. Yahia, and A. A. Al-Ghamdi, "Enhanced the photocatalytic activity of Ni-doped ZnO thin films: morphological, optical and XPS analysis," *Superlattices and Microstructures*, vol. 94, pp. 108–118, 2016.

[27] Z. Sarteep, A. E. Pirbazari, and M. A. Aroon, "Silver doped TiO_2 nanoparticles: preparation, characterization and efficient degradation of 2,4-dichlorophenol under visible light," *Journal of Water and Environmental Nanotechnology*, vol. 1, no. 12, pp. 135–144, 2016.

[28] C. A. Castro, A. Jurado, D. Sissa, and S. A. Giraldo, "Performance of Ag-TiO_2 photocatalysts towards the photocatalytic disinfection of water under interior-lighting and solar-simulated light irradiations," *International Journal of Photoenergy*, vol. 2012, Article ID 261045, 10 pages, 2012.

[29] Y. Liu, C. Y. Liu, J. H. Wei, R. Xiong, C. X. Pan, and J. Shi, "Enhanced adsorption and visible-light-induced photocatalytic activity of hydroxyapatite modified Ag-TiO_2 powders," *Applied Surface Science*, vol. 256, no. 21, pp. 6390–6394, 2010.

[30] H. Li, X. Duan, G. Liu, and X. Liu, "Photochemical synthesis and characterization of Ag/TiO_2 nanotube composites," *Journal of Materials Chemistry*, vol. 43, no. 5, pp. 1669–1676, 2008.

[31] F. Zhang, Y. Zheng, Y. Cao et al., "Ordered mesoporous Ag-TiO_2-KIT-6 heterostructure: synthesis, characterization and photocatalysis," *Journal of Materials Chemistry*, vol. 19, no. 18, pp. 2771–2777, 2009.

[32] Z. Xiong, J. Ma, W. J. Ng, T. D. Waite, and X. S. Zhao, "Silver-modified mesoporous TiO_2 photocatalyst for water purification," *Water Research*, vol. 45, no. 5, pp. 2095–2103, 2011.

[33] B. Naik, C. H. Manoratne, A. Chandrashekhar, A. Iyer, V. S. Prasad, and N. N. Ghosh, "Preparation of TiO_2, Ag-doped TiO_2 nanoparticle and TiO_2-SBA-15 nanocomposites using simple aqueous solution-based chemical method and study of their photocatalytical activity," *Journal of Experimental Nanoscience*, vol. 8, no. 4, pp. 462–479, 2013.

[34] Y. H. Teow, A. L. Ahmad, J. K. Lim, and B. S. Ooi, "Preparation and characterization of PVDF/TiO_2 mixed matrix membrane via in situ colloidal precipitation method," *Desalination*, vol. 295, pp. 61–69, 2012.

[35] M. A. Mohamed, W. N. W. Salleh, J. Jaafar et al., "Physicochemical characteristic of regenerated cellulose/N-doped TiO_2 nanocomposite membrane fabricated from recycled newspaper with photocatalytic activity under UV and visible light irradiation," *Chemical Engineering Journal*, vol. 284, pp. 202–215, 2016.

[36] T. Hwang, J. S. Oh, W. Yim et al., "Ultrafiltration using graphene oxide surface-embedded polysulfone membranes," *Separation and Purification Technology*, vol. 166, pp. 41–47, 2016.

[37] Y. Yang, H. Zhang, P. Wang, Q. Zheng, and J. Li, "The influence of nano-sized TiO_2 fillers on the morphologies and properties of PSF UF membrane," *Journal of Membrane Science*, vol. 288, no. 1-2, pp. 231–238, 2007.

[38] L. Daniel, H. Nagai, N. Yoshida, and M. Sato, "Photocatalytic activity of vis-responsive Ag-nanoparticles/TiO_2 composite thin films fabricated by molecular precursor method (MPM)," *Catalysts*, vol. 3, no. 3, pp. 625–645, 2013.

[39] N. Ma, Y. Zhang, X. Quan, X. Fan, and H. Zhao, "Performing a microfiltration integrated with photocatalysis using an Ag-TiO_2/HAP/Al_2O_3 composite membrane for water treatment: Evaluating effectiveness for humic acid removal and antifouling properties," *Water Research*, vol. 44, no. 20, pp. 6104–6114, 2010.

[40] Z. Xu, S. Ye, G. Zhang et al., "Antimicrobial polysulfone blended ultrafiltration membranes prepared with Ag/Cu_2O hybrid nanowires," *Journal of Membrane Science*, vol. 509, pp. 83–93, 2016.

[41] J. García-Serrano, E. Gómez-Hernández, M. Ocampo-Fernández, and U. Pal, "Effect of Ag doping on the crystallization and phase transition of TiO_2 nanoparticles," *Current Applied Physics*, vol. 9, no. 5, pp. 1097–1105, 2009.

[42] X. Li, K. Peng, H. Chen, and Z. Wang, "TiO_2 nanoparticles assembled on kaolinites with different morphologies for efficient photocatalytic performance," *Scientific Reports*, vol. 8, no. 1, article 11663, 2018.

[43] Q. Wang, C. Yang, G. Zhang, L. Hu, and P. Wang, "Photocatalytic Fe-doped TiO_2/PSF composite UF membranes: characterization and performance on BPA removal under visible-light irradiation," *Chemical Engineering Journal*, vol. 319, pp. 39–47, 2017.

[44] Q. Wang, G. S. Zhang, Z. S. Li, S. Deng, H. Chen, and P. Wang, "Preparation and properties of polyamide/titania composite nanofiltration membrane by interfacial polymerization," *Desalination*, vol. 352, pp. 38–44, 2014.

[45] K. Fischer, M. Grimm, J. Meyers, C. Dietrich, R. Gläser, and A. Schulze, "Photoactive microfiltration membranes via directed synthesis of TiO_2 nanoparticles on the polymer surface for removal of drugs from water," *Journal of Membrane Science*, vol. 478, pp. 49–57, 2015.

[46] H. Song, J. Shao, J. Wang, and X. Zhong, "The removal of natural organic matter with LiCl-TiO_2-doped PVDF membranes by integration of ultrafiltration with photocatalysis," *Desalination*, vol. 344, pp. 412–421, 2014.

[47] C. P. Athanasekou, N. G. Moustakas, S. Morales-Torres et al., "Ceramic photocatalytic membranes for water filtration under UV and visible light," *Applied Catalysis B: Environmental*, vol. 178, pp. 12–19, 2015.

[48] C. P. Athanasekou, S. Morales-Torres, V. Likodimos et al., "Prototype composite membranes of partially reduced graphene oxide/TiO_2 for photocatalytic ultrafiltration water treatment under visible light," *Applied Catalysis B: Environmental*, vol. 158-159, pp. 361–372, 2014.

[49] R. Goei, Z. Dong, and T. T. Lim, "High-permeability pluronic-based TiO_2 hybrid photocatalytic membrane with hierarchical porosity: fabrication, characterizations and performances," *Chemical Engineering Journal*, vol. 228, pp. 1030–1039, 2013.

[50] X.-F. Sun, J. Qin, P.-F. Xia et al., "Graphene oxide-silver nanoparticle membrane for biofouling control and water purification," *Chemical Engineering Journal*, vol. 281, pp. 53–59, 2015.